Submitted, 2005 Conference on Decision and Control (CDC)
http://www.cds.caltech.edu/~murray/papers/2005k_hmd05-cdc.html

A Control-Oriented Analysis of Bio-inspired Visuomotor Convergence[1]

J. Sean Humbert†
Richard M. Murray and Michael H. Dickinson
Division of Engineering and Applied Science
California Institute of Technology
Pasadena, CA 91125
†Corresponding Author: jshumber@cds.caltech.edu

***Abstract*— Insects exhibit unparalleled and incredibly robust flight dynamics in the face of uncertainties. A fundamental principle contributing to this amazing behavior is rapid processing and convergence of visual sensory information to flight motor commands via spatial wide-field integration, accomplished by motion pattern sensitive interneurons in the lobula plate portion of the visual ganglia. Within a control-theoretic framework, a model for wide-field integration of retinal image flow is developed, establishing the connection between image flow kernels (retinal motion pattern sensitivities) and the feedback terms they represent. It is demonstrated that the proposed output feedback methodology is sufficient to give rise to experimentally observed navigational heuristics as the centering and forward speed regulation responses exhibited by honeybees.**

I. INTRODUCTION

Prevalent in many natural sensory systems is the phenomenon of sensorimotor convergence, wherein signals from arrays of spatially distributed and differentially tuned sensors converge in vast number onto motor neurons responsible for controlling locomotive behavior. A prime example occurs in the processing of retinal image pattern movement (optic flow) by the visuomotor systems of insects. Insect visual systems encode optic flow by combining motion estimates from arrays of local motion detectors in a way that preserves the spatial layout of the retina [1]. This sensory information is parsed by wide-field motion sensitive interneurons (tangential cells, or LPTCs) in the lobula plate section of the visual ganglia, as shown in (Figure 3A). The output of these neurons synapse in the motor control centers, creating a sensory processing stage which spatially integrates the optic flow [2]. This visuomotor convergence technique, spatial wide-field integration, is used by insects to extract behaviorally-relevant information from optic flow patterns to modulate the kinematics of flight [3].

Since optic flow was first recognized as a critical source of information [4], there has been considerable interest in adapting this type of sensory system for bio-inspired autonomous navigation. Efforts have focused on utilizing one or more properties of optic flow to provide navigational cues [5]. Examples include corridor navigation based on balancing average lateral image velocities on wheeled robots, obstacle avoidance via saccading away from regions with high image velocities, and optic flow based estimates of depth [6]. In a more traditional approach, LPTC-based processing models have been investigated as estimators for vehicle kinematic states directly from observed optic flow [7], as tangential cell sensitivity maps show similarities to flow fields that correspond to egomotion [8].

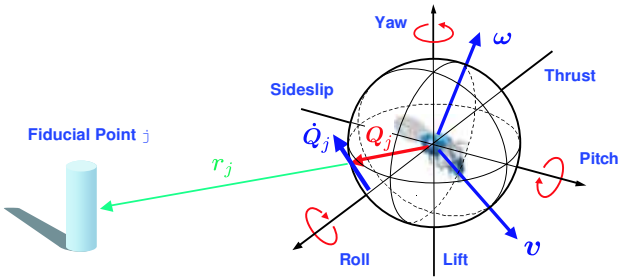

Fig. 1. Motion Parallax Field Definitions

In this paper we propose a more general functional role for wide-field sensitive neurons in navigation and flight control as well as a novel methodology for utilizing optic flow sensory information in bio-inspired applications. We show how the spatial harmonics of planar optic flow, extracted with motion-pattern sensitive kernels representing LPTCs (Figure 3B), correspond to feedback terms which can be used to stabilize the different navigational modes of flight. Section II develops the equations that govern spherical motion parallax fields of three dimensional environments. A model for wide-field integration of planar retinal image flow is presented in Section III, and the connection between image flow kernels and the output feedback terms they represent is established. In Section IV the concept of *balancing* or *shaping* the object nearness function through feedback of wide-field integration outputs is introduced, and stabilization of forward speed regulation and obstacle avoidance behaviors is demonstrated via simulations with planar wheeled robot dynamics.

II. A CONTINUOUS FIELD MODEL OF OPTIC FLOW

In the idealized case, the retinal image motion field is a function of the motion of the vantage point along with the spatial structure and distribution of objects (or fiducial points) in the environment. The basic set of equations that specify a general discrete optic flow field for an environment composed of $j = 1 \ldots N$ rigid fiducial points (Figure 1) were

[1] Partial support for this work was provided by AFOSR under grant F30602-01-2-0558 and ARO under grant DAAD19-03-D-0004

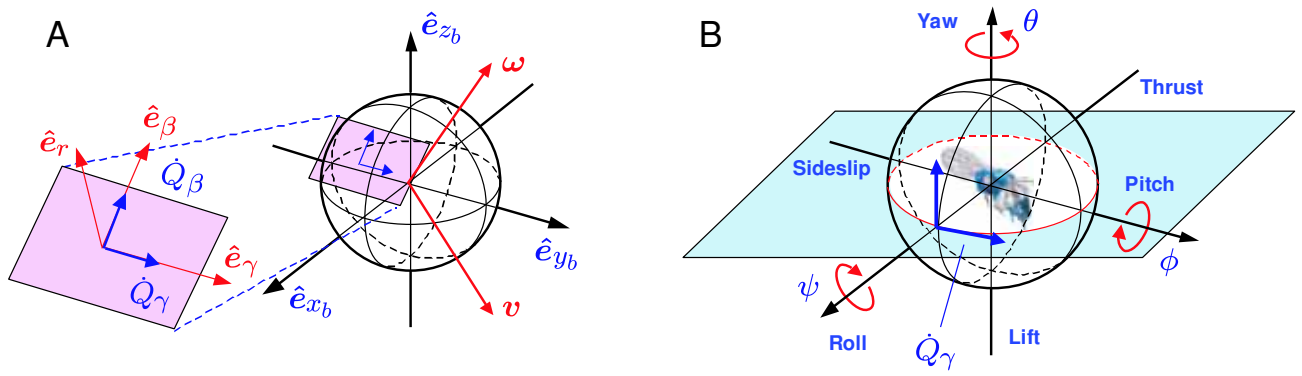

Fig. 2. Pitch-Altitude Optic Flow Definitions

developed in [9]:

$$\dot{\boldsymbol{Q}}_j \;=\; -\boldsymbol{\omega}\times\boldsymbol{Q}_j - \frac{1}{r_j}\left[\boldsymbol{v} - \langle \boldsymbol{v}, \boldsymbol{Q}_j\rangle \boldsymbol{Q}_j\right]. \qquad (1)$$

A fiducial point j is located with respect to the vantage point (the origin of the body frame coordinate system b) by a vector $\boldsymbol{r}_j \in \mathbb{R}^3$ with magnitude $r_j = \|\boldsymbol{r}_j\|$ along marker $\boldsymbol{Q}_j = \boldsymbol{r}_j/r_j$. The motion parallax $\dot{\boldsymbol{Q}}_j$ induced by body frame angular and linear velocities $(\boldsymbol{\omega}, \boldsymbol{v})$ with respect to fiducial point j is defined as the time derivative of the marker $\boldsymbol{Q}_j \in S^2$. Collectively, the set of markers and motion parallax vectors $\{\boldsymbol{Q}_j, \dot{\boldsymbol{Q}}_j, j = 1\ldots N\}$ compose a general spatially-discrete optic flow field.

Equation (1) is a composition of two critical pieces of information: the vantage point motion, useful for the flight stabilization task, and the spatial distribution of objects in the environment, which is useful for navigation tasks such as obstacle avoidance and terrain following. As noted above, it is presumed that insect visual systems extract these types of control-relevant information by parsing this field via wide-field pattern sensitive neurons. Our analysis of this process will will require the development of a control-oriented version of the 3-D motion parallax field (1), or more specifically a body-frame-relative spherical coordinate representation $\dot{\boldsymbol{Q}} = \dot{Q}_r\ \hat{\boldsymbol{e}}_r + \dot{Q}_\gamma\ \hat{\boldsymbol{e}}_\gamma + \dot{Q}_\beta\ \hat{\boldsymbol{e}}_\beta$ with a continuous formulation of the spatial distribution of objects in the environment and kinematics $\boldsymbol{\omega}, \boldsymbol{v}$ expressed in body frame coordinates (Figure 2A). For a continuous representation of the spatial distribution (rigidity hyp?) of the environment, the set of distances to the fiducial points $\{r_i, i = 1\ldots N\}$ becomes a function of the azimuth and elevation angles $r(\gamma,\beta) : [0, 2\pi] \times [0, \pi] \mapsto (0, \infty)$. Implicit to this definition, $r(\gamma,\beta)$ also depends on the particular environment as well as the vantage point configuration (position and orientation) within that environment. We expect this function to take on values from $(0, \infty)$ and contain discontinuities, especially in a cluttered object field. By explicitly restricting contact $r(\gamma,\beta) = 0$, we ensure that the reciprocal $\mu(\gamma,\beta) = 1/r(\gamma,\beta)$, defined as the *nearness*, is a bounded, piecewise continuous function with a finite (countable) number of discontinuities and is restricted to the space of square integrable functions $L_2([0, 2\pi] \times [0, \pi]) = \left\{f : [0, 2\pi] \times [0, \pi] \to \mathbb{R} : \int_0^{2\pi}\int_0^{\pi} |f(\gamma,\beta)|^2\, d\gamma d\beta < \infty\right\}$. If we express the vantage point kinematics and general unit marker $\boldsymbol{Q}(\gamma,\beta) \in S^2$ in body frame rectangular coordinates

$$\begin{aligned}
\boldsymbol{\omega} &= \dot{\psi}\,\hat{\boldsymbol{e}}_{x_b} + \dot{\phi}\,\hat{\boldsymbol{e}}_{y_b} + \dot{\theta}\,\hat{\boldsymbol{e}}_{z_b}\\
\boldsymbol{v} &= \dot{x}_b\,\hat{\boldsymbol{e}}_{x_b} + \dot{y}_b\,\hat{\boldsymbol{e}}_{y_b} + \dot{z}_b\,\hat{\boldsymbol{e}}_{z_b}\\
\boldsymbol{Q} &= \cos\gamma\cos\beta\,\hat{\boldsymbol{e}}_{x_b} + \sin\gamma\cos\beta\,\hat{\boldsymbol{e}}_{y_b} + \sin\beta\,\hat{\boldsymbol{e}}_{z_b},
\end{aligned}$$

the motion parallax field (1) becomes

$$\dot{\boldsymbol{Q}} \;=\; \hat{\boldsymbol{Q}}\boldsymbol{\omega} - \mu\left(I - \boldsymbol{Q}\boldsymbol{Q}^T\right)\boldsymbol{v} \qquad (2)$$

where

$$\hat{\boldsymbol{Q}} \;=\; \begin{pmatrix} 0 & -\sin\beta & \sin\gamma\cos\beta \\ \sin\beta & 0 & -\cos\gamma\cos\beta \\ -\sin\gamma\cos\beta & \cos\gamma\cos\beta & 0 \end{pmatrix}$$

is the matrix representation of the linear operator $\boldsymbol{\omega} \mapsto -\boldsymbol{\omega}\times\boldsymbol{Q}$. To put (2) into spherical coordinates, we apply the transformation from rectangular coordinates

$$T \;=\; \begin{pmatrix} \cos\gamma\cos\beta & \sin\gamma\cos\beta & \sin\beta \\ -\sin\gamma & \cos\gamma & 0 \\ -\cos\gamma\sin\beta & -\sin\gamma\sin\beta & \cos\beta \end{pmatrix}$$

to arrive at our goal of a control-oriented representation $\dot{\boldsymbol{Q}} = \dot{Q}_r\,\hat{\boldsymbol{e}}_r + \dot{Q}_\gamma\,\hat{\boldsymbol{e}}_\gamma + \dot{Q}_\beta\,\hat{\boldsymbol{e}}_\beta$ of (1):

$$\dot{\boldsymbol{Q}} \;=\; A\boldsymbol{\omega} + \mu B\boldsymbol{v}. \qquad (3)$$

The matricies $A = T\hat{\boldsymbol{Q}}$ and $B = -T\left(I - \boldsymbol{Q}\boldsymbol{Q}^T\right)$ are given by

$$\begin{aligned}
A &= \begin{pmatrix} 0 & 0 & 0 \\ \sin\beta\cos\gamma & \sin\beta\sin\gamma & -\cos\beta \\ \sin\gamma & \cos\gamma & 0 \end{pmatrix}\\
B &= \begin{pmatrix} 0 & 0 & 0 \\ -\sin\gamma & \cos\gamma & 0 \\ -\sin\beta\cos\gamma & -\sin\beta\sin\gamma & \cos\beta \end{pmatrix}.
\end{aligned}$$

A priori we expect $\dot{Q}_r = 0$ as the translational contribution to (1) is a normal projection. It is further assumed that the kinematics are bounded, piecewise-continuous functions of time, hence the instantaneous motion parallax components $\dot{Q}_\gamma$ and $\dot{Q}_\beta$ are restricted to $L_2([0, 2\pi] \times [0, \pi])$.

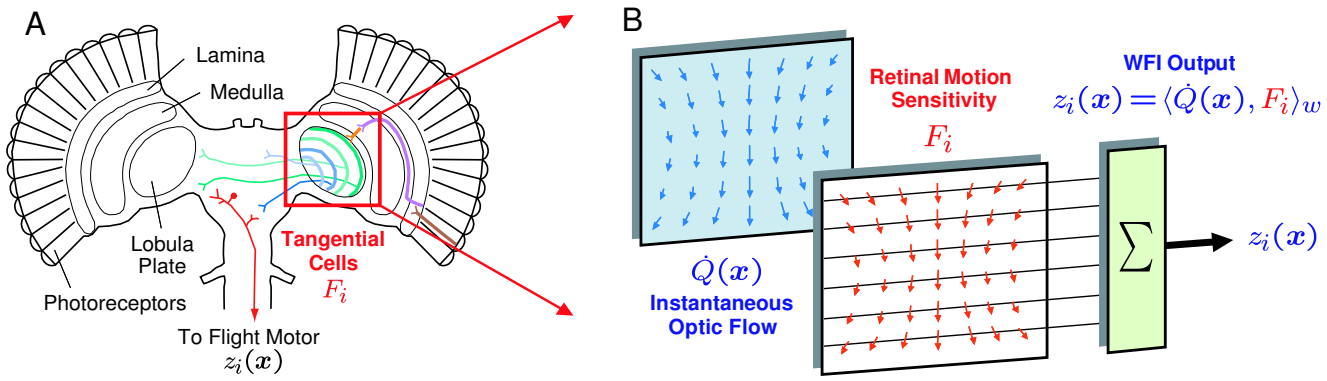

Fig. 3. (A) Visuomotor system of insects. Wide-field retinal motion sensitive interneurons (tangential cells) parse spatially-preserved visual information and transmit it to motor control centers. (B) WFI processing model. Spatial modes of optic flow are extracted by retinal motion sensitivity kernels.

For planar guidance and navigation applications where rigid body motion is restricted to 3 DOF (planar translation with yaw rotation) we will consider the special case of the tangential optic flow component $\dot{Q}_\gamma$ defined by the intersection of S^2 and the plane $\beta = 0$, as shown in Figure 2B. Under these conditions, the optic flow on a ring-shaped sensor becomes a 2π-periodic function of the vehicle-referred viewing angle γ, that is $\dot{Q}_\gamma = -\dot{\theta} + \mu(\gamma, 0)\,(\dot{x}_b \sin\gamma - \dot{y}_b \cos\gamma)$. Clearly for fixed t, $\mu(\gamma, 0) \in L_2[0, 2\pi]$ and therefore $\dot{Q}_\gamma \in L_2[0, 2\pi]$. For notational convenience in the remainder of the paper we will refer to the planar nearness function for the environment of interest as $\mu(\gamma)$ or more appropriately as $\mu(\gamma, \boldsymbol{x})$, noting the dependence on components of the *state* of the insect (or vehicle), $\boldsymbol{x}(t)$, which without specifying the coordinate frame is simply the inertial configuration (position and orientation) and associated linear and angular velocities. In addition we will drop the γ subscript and refer to the planar motion parallax as $\dot{Q}$, or $\dot{Q}(\gamma, \boldsymbol{x})$, also noting the dependence on the vehicle's state:

$$\dot{Q}(\gamma, \boldsymbol{x}) \;=\; -\dot{\theta} + \mu(\gamma, \boldsymbol{x})\,(\dot{x}_b \sin\gamma - \dot{y}_b \cos\gamma)\,. \quad (4)$$

III. A Model for Wide-Field Integration Processing of Ideal Planar Optic Flow

For this treatment we will represent the lobula plate tangential cells (or dorsal and ventral pairs as may be appropriate) by a weight $F_i(\gamma) \in L_2[0, 2\pi]$, which models their sensitivity to various motion patterns. Weights $F_i(\gamma)$ are essentially a spatially distributed set static gains which are applied to the output at the corresponding local motion detectors at retinal positions γ. Through appropriate choices of $F_i(\gamma)$, we are interested in characterizing the available information relevant for use in closed loop feedback. We expect these weighting functions to be piecewise continuous and square-integrable, hence the restriction to the function space $L_2[0, 2\pi]$. For this initial analysis we will also assume that optic flow estimation processing (photoreceptors and local motion detectors) have negligible dynamics, that is wide-field spatial integration (henceforth WFI) can be modeled in entirety by a transformation W, representing a spatial integration against the motion parallax kernel (4), which acts on elements $F_i(\gamma)$ to produce a sensor output signal z_i, hence $W : F_i \in L_2[0, 2\pi] \mapsto z_i \in \mathbb{R}$. The transformation W defined by $z_i = WF_i$ can be represented as a linear functional using the inner product structure available on $L_2[0, 2\pi]$:

$$z_i(\boldsymbol{x}) \;=\; \langle \dot{Q}, F_i \rangle_w \;=\; \frac{1}{\pi} \int_0^{2\pi} \dot{Q}(\gamma, \boldsymbol{x}) \cdot F_i(\gamma)\; d\beta. \quad (5)$$

The inner product (5) has been defined with a factor of $1/\pi$ to be compatible with the typical Fourier harmonic component definition so that later notation is simplified.

A. Characterization of WFI Sensory Outputs for Planar Optic Flow

We are interested in characterizing the set of all possible sensory outputs available within this model and their dependency on vehicle motion and spatial distribution of objects in the environment. Since $L_2[0, 2\pi]$ is a Hilbert space, and more specifically a complete, separable inner product space, a countably infinite orthonormal basis $\{\phi_n(\gamma)\}$ exists. For fixed t, $\dot{Q}(\gamma, \boldsymbol{x}) \in L_2[0, 2\pi]$, therefore we can expand it in a generalized Fourier series $\dot{Q}(\gamma, \boldsymbol{x}) = \sum_n^\infty \langle \dot{Q}(\gamma, \boldsymbol{x}), \phi_n(\gamma) \rangle\, \phi_n(\gamma)$. If we use trigonometric Fourier series (basis fcn expl), the orthonormal basis $\Phi = \{\phi_n(\gamma)\}$ under the inner product (5) is

$$\begin{aligned} \Phi \;=\; & \{1/\sqrt{2}\} \cup \{\cos n\gamma : n = 1, 2, \ldots\} \\ & \cup \{\sin n\gamma : n = 1, 2, \ldots\}, \end{aligned}$$

and the expansion becomes

$$\dot{Q}(\gamma, \boldsymbol{x}) = \frac{a_0(\boldsymbol{x})}{2} + \sum_{n=1}^{\infty} a_n(\boldsymbol{x}) \cos n\gamma + \sum_{n=1}^{\infty} b_n(\boldsymbol{x}) \sin n\gamma,$$

where the state-dependent spatial harmonics of the motion parallax field are defined as

$$\begin{aligned} a_0(\boldsymbol{x}) \;&=\; \langle \dot{Q}, 1/\sqrt{2} \rangle_w \;&=\; \tfrac{1}{\pi} \textstyle\int_0^{2\pi} \dot{Q}(\gamma, \boldsymbol{x})/\sqrt{2}\; d\gamma \\ a_n(\boldsymbol{x}) \;&=\; \langle \dot{Q}, \cos n\gamma \rangle_w \;&=\; \tfrac{1}{\pi} \textstyle\int_0^{2\pi} \dot{Q}(\gamma, \boldsymbol{x}) \cos n\gamma\; d\gamma \\ b_n(\boldsymbol{x}) \;&=\; \langle \dot{Q}, \sin n\gamma \rangle_w \;&=\; \tfrac{1}{\pi} \textstyle\int_0^{2\pi} \dot{Q}(\gamma, \boldsymbol{x}) \sin n\gamma\; d\gamma. \end{aligned}$$

With some manipulations, we can re-write these expressions in terms of the vehicle state $\boldsymbol{x}(t)$ and the spatial harmonics

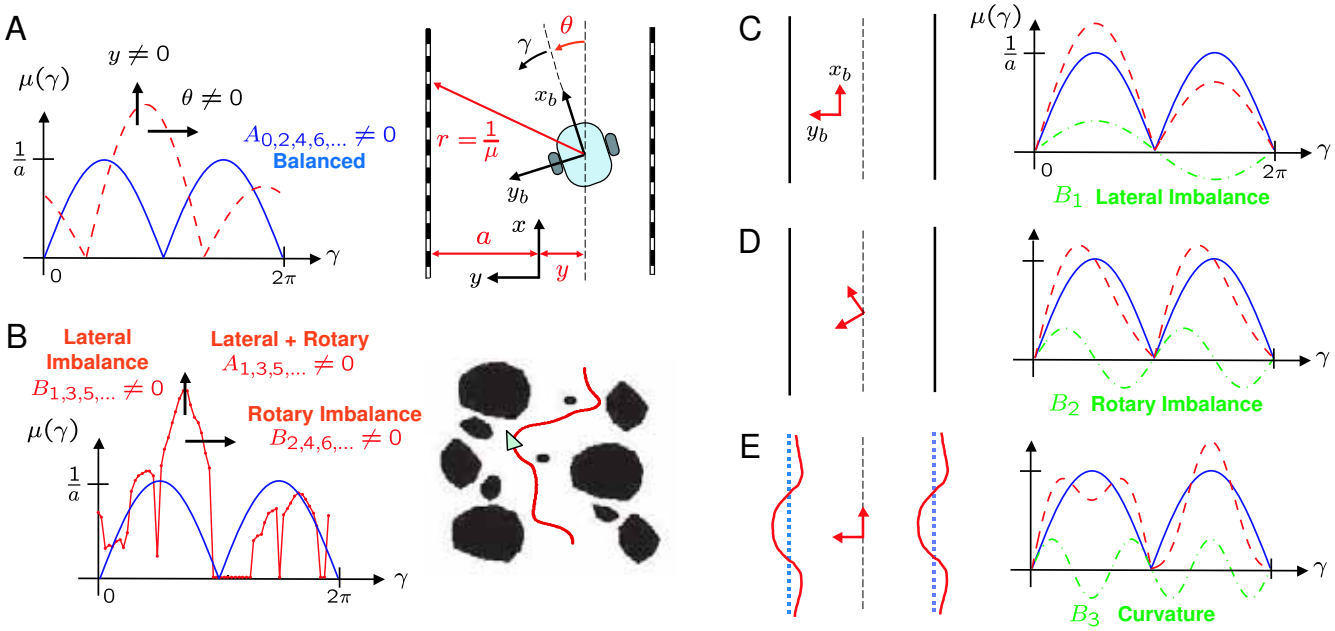

Fig. 4. Connections between WFI outputs and μ. (A) Planar tunnel geometry and lateral/rotational perturbations of μ (B) μ-shaping in environments with higher order spatial structure

$\{A_0(\boldsymbol{x}), A_k(\boldsymbol{x}), B_k(\boldsymbol{x}) : k = 1, 2, \ldots\}$ of the nearness function $\mu(\beta, \boldsymbol{x})$:

$$\begin{aligned} a_0(\boldsymbol{x}) &= (-\dot{\theta} + \dot{x}_b B_1 - \dot{y}_b A_1)/\sqrt{2} \\ a_n(\boldsymbol{x}) &= \frac{\dot{x}_b}{2}(-B_{n-1} + B_{n+1}) - \frac{\dot{y}_b}{2}(A_{n-1} + A_{n+1}) \\ b_n(\boldsymbol{x}) &= \frac{\dot{x}_b}{2}(A_{n-1} - A_{n+1}) - \frac{\dot{y}_b}{2}(B_{n-1} + B_{n+1}), \end{aligned} \tag{6}$$

where

$$\mu(\gamma, \boldsymbol{x}) = \frac{A_0(\boldsymbol{x})}{2} + \sum_{k=1}^{\infty} A_k(\boldsymbol{x}) \cos n\gamma + \sum_{k=1}^{\infty} B_k(\boldsymbol{x}) \sin n\gamma.$$

Now, under the interpretation

$$\begin{aligned} W\Phi &= \{a_0(\boldsymbol{x})\} \cup \{a_n(\boldsymbol{x}) : n = 1, 2, \ldots\} \\ &\quad \cup \{b_n(\boldsymbol{x}) : n = 1, 2, \ldots\}, \end{aligned}$$

the equations (6) define the action of the linear transformation $W : L_2[0, 2\pi] \mapsto \mathbb{R}$ on a basis Φ for the domain, and as such uniquely characterize the set of all possible wide-field integration sensory outputs.

B. Interpretation of WFI Outputs

The relationships in (6) define how WFI outputs depend on vehicle motion $(\dot{x}_b, \dot{y}_b, \dot{\theta})$ and object nearness $\{A_0, A_k, B_k : k = 1, 2, \ldots\}$ with respect to the vantage point position and orientation, however the intuition required to utilize them in closed loop feedback is not readily apparent. As a motivational example, we consider a planar tunnel geometry (Figure 4A), which provides a reasonable approximation to flight between two obstacles. In this case the nearness function $\mu(\gamma, \boldsymbol{x})$ can be expressed in closed form as a function of the lateral position y, body frame orientation θ, and the tunnel half-width a:

$$\mu(\gamma, \boldsymbol{x}) = \begin{cases} \frac{\sin(\gamma+\theta)}{a-y} & 0 \leq \gamma + \theta < \pi \\ -\frac{\sin(\gamma+\theta)}{a+y} & \pi \leq \gamma + \theta < 2\pi \end{cases}. \tag{7}$$

For a perfectly centered vehicle $(y, \theta) = (0, 0)$, (7) reduces to $|\sin\gamma|/a$, which has a Fourier series expansion

$$\mu(\gamma, \boldsymbol{x})|_{y,\theta=0} = \frac{2}{a\pi} - \sum_{k=2,4,6,\ldots}^{\infty} \frac{4}{a\pi(k^2-1)} \cos k\gamma. \tag{8}$$

Note that the expansion is composed of a DC component and even cosine harmonics $\{A_k : k = 0, 2, 4, \ldots\}$ of decreasing amplitude only. (8) represents the *balanced* or *equilibrium* nearness shape (Figure 4A), as it corresponds to flight along the centerline of the tunnel. For lateral and rotary displacements, the spatial harmonics of the perturbed nearness

TABLE I
INTERPRETATION OF μ SPATIAL FOURIER HARMONICS A_k,B_k

Mode	Balanced	General Tunnel	Imbalance
A_0	$\frac{2}{a\pi}$	$\frac{2a}{\pi(a^2-y^2)}$	-
A_1	0	$\frac{y \sin\theta}{(a^2-y^2)}$	Lateral + Rotary
B_1	0	$\frac{y \cos\theta}{(a^2-y^2)}$	Lateral
$A_{2,4,6,\ldots}$	$-\frac{4}{a\pi(k^2-1)}$	$-\frac{4a \cos k\theta}{\pi(a^2-y^2)(k^2-1)}$	-
$B_{2,4,6,\ldots}$	0	$-\frac{4a \sin k\theta}{\pi(a^2-y^2)(k^2-1)}$	Rotary
$A_{3,5,7,\ldots}$	0	0	Lateral + Rotary
$B_{3,5,7,\ldots}$	0	0	Lateral

function are computed in Table I. From the linearizations about the point $(y, \theta) = (0, 0)$ it is clear that the B_1 harmonic provides an estimate of the lateral displacement (Figure 4C) while the B_2 harmonic provides an estimate of the rotary displacement (Figure 4D). These results can be generalized to environments with more complicated spatial structure (Figure 4B,E); nonzero $B_{1,3,5,\ldots}$ correspond to a lateral imbalance, $B_{2,4,6,\ldots}$ to a rotary imbalance, and $A_{1,3,5,\ldots}$ are coupling terms for a lateral plus a rotary imbalance.

IV. μ-SHAPING VIA STATIC OUTPUT FEEDBACK

In this section we demonstrate the utility of WFI sensory outputs (6) through coupling with planar flight dynamics via static output feedback (Figure 5). The WFI operator is used

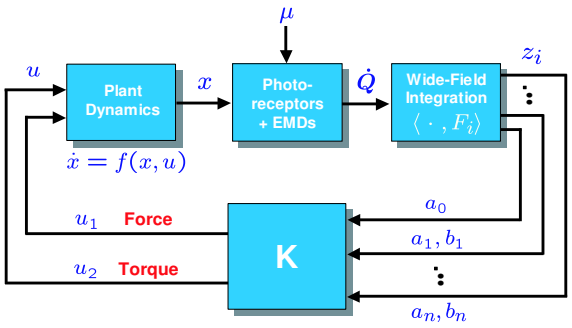

Fig. 5. Closed loop WFI output feedback

to decompose the optic flow into spatial harmonics (6), and force and torque control inputs u_1, u_2 are computed as static combinations

$$u_i = K^a_{i0}\, a_0 + \sum_{j=1}^{n} K^a_{ij}\, a_j + K^b_{ij}\, b_j, \tag{9}$$

which correspond to motion sensitivity functions

$$F_{u_i} = K^a_{i0} + \sum_{j=1}^{n} K^a_{ij} \cos j\gamma + K^b_{ij} \sin j\gamma. \tag{10}$$

For analysis and simulation purposes we will consider rolling or wheeled vehicles of the unicycle type (Figure 4A), subject to the nonholonomic constraint

$$\dot{x} \sin\theta - \dot{y} \cos\theta \;=\; 0, \tag{11}$$

which enforces $\dot{y}_b = 0$. It is assumed that the two wheels providing continuous contact with the ground are driven independently, and the vehicle center of mass is located at the midpoint along the axis between them. In the inertial configuration (x, y, θ) the kinematic and dynamic equations describing the motion are

$$\begin{aligned} \dot{x} &= v \cos\theta \\ \dot{y} &= v \sin\theta \\ m\dot{v} &= \frac{1}{r_w}(T_s + T_p) \\ J\ddot{\theta} &= \frac{r_0}{r_w}(T_s - T_p), \end{aligned} \tag{12}$$

where starboard and port wheel torques are denoted by T_s and T_p, r_0 and r_w denote the vehicle width and wheel radius, and the vehicle mass and rotational inertia are given by m and J.

A. Linear Analysis

In the initial version of this work presented here, the intent is to show feasibility of the proposed output feedback methodology, hence a linearized control design which guarentees local asymptotic stability of speed regulation and obstacle avoidance responses will be discussed. It will be useful to introduce the following state and input definitions $v = \dot{x}_b$, $u_1 = (T_s + T_p)/r_w$, and $u_2 = r_0(T_s - T_p)/r_w$. Assuming small states (other than v) and control inputs, the linearized equations of motion for a centerline flight trajectory become

$$\begin{aligned} m\dot{v} &= u_1 \\ \dot{y} &= v_0\theta \\ J\ddot{\theta} &= u_2 \end{aligned} \tag{13}$$

Equation 14 shows the resulting linearization $z(\boldsymbol{x}) = z(\boldsymbol{x}_0) + \sum_i \frac{\partial z}{\partial x_i}(\boldsymbol{x}_0)\,(x_i - x_{i0})$, of outputs a_0, a_1, b_1 and a_2 for the planar tunnel with respect to the kinematic variables $\boldsymbol{x} = [\; v \;\; y \;\; \dot{y} \;\; \theta \;\; \dot{\theta} \;]'$ along a reference trajectory $\boldsymbol{x}_0 = [\; v_0 \;\; 0 \;\; 0 \;\; 0 \;\; 0 \;]'$, corresponding to a centerline flight path at a constant velocity v_0.

$$\begin{pmatrix} z_{b_1} \\ z_{a_0} \\ z_{a_1} \\ z_{a_2} \end{pmatrix} = \begin{pmatrix} \frac{8}{3\pi a} & 0 & 0 & 0 \\ 0 & \frac{v_0}{\sqrt{2}a^2} & 0 & -\sqrt{2} \\ 0 & 0 & \frac{4v_0}{3\pi a} & 0 \\ 0 & -\frac{v_0}{4a^2} & 0 & 0 \end{pmatrix} \begin{pmatrix} v \\ y \\ \theta \\ \dot{\theta} \end{pmatrix} \tag{14}$$

Notice in (13) that the v dynamics are decoupled from the y, θ dynamics and in (14) the linearized b_1 output is a function of v only and the linearized a_0, a_1, a_2 outputs are functions of $y, \theta, \dot{\theta}$. Hence, with the linearized system we can effectively decouple the control problem into the *clutter* (forward speed regulation) response and the *centering* (obstacle avoidance) response.

For the forward speed regulation task, we define a reference forward velocity r and corresponding scaling factor N and close the loop by setting the thrust input

$$u_1 \;=\; K^b_{11}(Nr - b_1), \tag{15}$$

corresponding to the motion sensitivity function

$$F_{u_1}(\gamma) \;=\; K^b_{11} \sin\gamma. \tag{16}$$

With $r = v_0$, choose $N = 8/(3\pi a)$ for zero steady-state error, and the linearized closed loop dynamics become

$$\dot{v} \;=\; -\frac{N}{m} K^b_{11}(v - v_0).$$

One can easily verify that with $K^b_{11} > 0$ local stability is achieved.

As for the centering and obstacle avoidance response, a quick check of the controllability and observability matricies shows that the linearized system is completely controllable

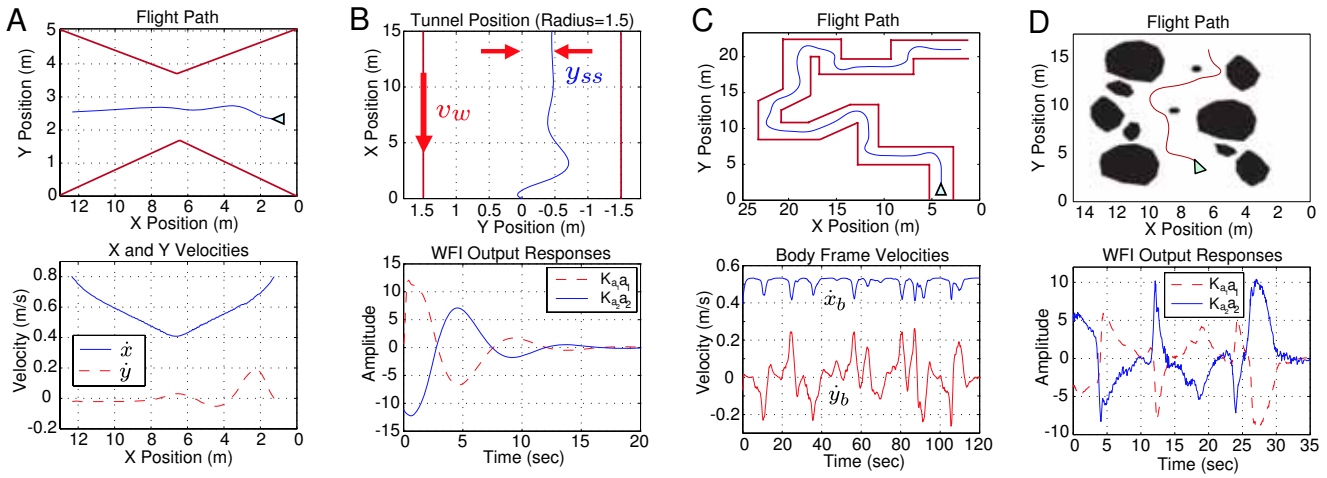

Fig. 6. Simulations of WFI-based navigation. (A) Clutter response for a converging-diverging tunnel (B) Centering response with a moving wall (C) Corridor navigation (D) Obstacle field navigation

and observable as long as $v_0 \neq 0$. Therefore, due to the coupling of the lateral to the rotational dynamics through the $v_0\theta$ term in (13), it is possible to accomplish stabilization of both modes via static output feedback through the torque input, taken to be

$$u_2 \quad = \quad K^a_{20}a_0 + K^a_{21}a_1 + K^a_{22}a_2, \qquad (17)$$

corresponding to the motion sensitivity function

$$F_{u_2}(\gamma) \quad = \quad K^a_{20} + K^a_{21}\cos\gamma + K^a_{22}\cos 2\gamma. \qquad (18)$$

The natural dynamics contain only inertial and viscous terms, therefore to achieve a stable centering/obstacle avoidance response, we require $K^a_{21} < 0$ for rotational stiffness and $K^a_{22} > 0$ for lateral stiffness. Additionally, rotational damping can be added with $K^a_{20} > 0$, however the linearization of the DC component a_0 of $\dot{Q}$ also has a lateral imbalance term (14), hence we further need the restriction $K^a_{22} > \sqrt{2}K^a_{20}$ to provide the lateral stiffness required for a stable centering response. This can be verified by the characteristic equation for the linearized closed loop dynamics

$$s^3 + \frac{K^a_{20}}{J}s^2 - \frac{8K^a_{21}v_0}{3J\pi a}s + \frac{v_0(K^a_{22} - \sqrt{2}K^a_{20})}{Ja^2} = 0 \qquad (19)$$

B. Simulation Results

We have constructed simulations based on the full nonlinear planar flight dynamics (12) to qualitatively compare the performance of the WFI control methodology to these experimental assays. Environments were defined as bitmaps, and the instantaneous optic flow was computed by estimating the depth at the current location and orientation at 60 equally-spaced circumferential points and combining it with the current kinematics according to (4). Force and torque control inputs are generated by taking the discrete inner product of the instantaneous optic flow with appropriately sampled versions of the motion sensitivity functions (16) and (18). Sensitivity gains K^a_{ij} and K^b_{ij} used in the simulation were chosen based on the the performance index of maximizing the bandwidth of the slow (lateral) mode in the linearized closed loop system (19). Figure 6A shows the centering/clutter responses for the hovercraft navigating a converging-diverging tunnel; the forward speed is indeed proportional to tunnel width, as seen in [10].

The closed loop behavior of this output feedback methodology was also evaluated in more complicated environments. Using the same feedback structure and gains, the vehicle was directed to navigate a complicated corridor (Figure 6C) and an obstacle field (Figure 6D). Body velocities are shown for the corridor, and the response of the first two cosine harmonics of the optic flow are shown for the obstacle field.

C. Navigation of General Environments

In this section we consider the interpretation of WFI static feedback in the context of the output regulation problem; that is, regulating or shaping the spatial harmonic content of the nearness μ. Recall the balanced nearness function (8) for the infinite tunnel, which was composed of DC and even (negative) cosine harmonics $\{A_0, A_k, k = 1, 2, \ldots\}$. In the case of a more general obstacle field, we can choose this as our desired μ shape, and through feedback of WFI outputs we can filter out unwanted spatial content. The fundamental sine harmonic of the 1-D motion parallax field,

$$b_1 \quad = \quad \frac{\dot{x}_b}{2}(A_0 - A_2),$$

is proportional to the desired spatial content, therefore provides an estimate of the forward speed $v = \dot{x}_b$, and can be used to maintain a pre-determined reference value as in (15). The speed setpoint is automatically reduced as the magnitudes of A_0 and A_2 increase, i.e. the obstacle field becomes increasingly cluttered.

The first two cosine harmonics of the motion parallax field,

$$\begin{aligned} a_0 &= -\sqrt{2}\dot{\theta} + \frac{\dot{x}_b}{\sqrt{2}} B_1 \\ a_1 &= \frac{\dot{x}_b}{2} B_2 \\ a_2 &= \frac{\dot{x}_b}{2}(-B_1 + B_3), \end{aligned}$$

are functions of even and odd sine harmonics B_k of the nearness function. Therefore, balancing the a_1 component contributes rotary stiffness to the loop and balancing the a_2 component contributes lateral stiffness (Figures 4B-4E) for a control system that is regulating about a fixed forward speed $v = \dot{x}_b$. In addition, balancing the DC component adds rotary damping to the loop. The closed loop behavior of this output feedback methodology was evaluated in more complicated environments. The vehicle was directed to navigate a complicated corridor (Figure 6C) and an obstacle field (Figure 6D). Body velocities are shown for the corridor, and the response of the first two cosine harmonics of the optic flow are shown for the obstacle field. The corrective torque for the lateral imbalance is supplied by a_2, and the dynamics are stabilized with the opposing rotational stiffness from a_1.

V. Conclusions

A control-oriented analytical model for spatial wide-field integration (WFI) of retinal image flow was developed. The model provides a unique characterization of information available for feedback from WFI sensory systems, and establishes the connection between global structure of optic flow (retinal motion sensitivity patterns) and the control-relevant information available for feedback.

The analysis presented suggests a more general functional role for wide-field sensitive neurons in navigation and flight control as well as a novel methodology for utilizing optic flow in bio-inspired applications. Rather than implementing wide-field integrators as direct estimators of kinematics or depth, it was shown how the spatial harmonics of planar optic flow, extracted with motion-pattern sensitive kernels, correspond to feedback terms which can be used to stabilize various reflexive behaviors. The proposed WFI output feedback methodology is shown to be equivalent to stabilizing the closed loop dynamics with respect to spatial perturbations from a balanced nearness function, and has the advantage of being computationally inexpensive as each required control input can be computed with an inner product of vectors on the order of 60 elements.

Planar flight stabilization and navigation in complicated environments has been demonstrated in simulation, and it is shown that the proposed methodology has sufficient complexity to give rise to experimentally observed navigational heuristics as the centering and forward speed regulation responses exhibited by honeybees.

References

[1] M. Egelhaaf and A. Borst, "Motion computation and visual orientation in flies," *Comp. Biochem. Phisiol.*, vol. 104A, pp. 659–673, 1993.

[2] A. Borst and J. Haag, "Neural networks in the cockpit of the fly," *J. Comp. Physiol. A*, vol. 188, pp. 419–437, 2002.

[3] M. Frye and M. Dickinson, "Fly flight: A model for the neural control of complex behavior," *Neuron*, vol. 32, pp. 385–388, 2001.

[4] J. Gibson, *The perception of the visual world*. Boston: Houghton Mifflin, 1950.

[5] G. Barrows, J. Chahl, and M. Srinivasan, "Biologically inspired visual sensing and flight control," *The Aeronautical Journal*, vol. 107, pp. 159–168, 2003.

[6] M. Franz and H. Mallot, "Biomimetic robot navigation," *Robotics and Autonomous Systems*, vol. 30, pp. 133–153, 2000.

[7] M. Franz, J. Chahl, and H. Krapp, "Insect-inspired estimation of egomotion," *Neural Computation*, vol. 16, pp. 2245–2260, 2004.

[8] H. Krapp, B. Hengstenberg, and R. Hengstenberg, "Dendritic structure and receptive-field organization of optic flow processing interneurons in the fly," *J. Neurophysiol.*, vol. 79, pp. 1902–1917, 1998.

[9] J. Koenderink and A. van Doorn, "Facts on optic flow," *Biol. Cybern.*, vol. 56, pp. 247–254, 1997.

[10] M. Srinivasan, S. Zhang, M. Lehrer, and T. Collet, "Honeybee navigation *en route* to the goal: visual flight control and odometry," *J. Exp. Biol.*, vol. 199, pp. 237–244, 1996.